Int. J. Electrochem. Sci., 17 **(2022)** Article Number: 220554, doi: 10.20964/2022.05.29

International Journal of
ELECTROCHEMICAL
SCIENCE
www.electrochemsci.org

Numerical Assessment of Heat Transfer on a PEM Fuel Cell Stack with Different Refrigeration Systems: Heat Source Management

C.E. Hernández-Herrera[1], *J. M. Sierra*[1,*], *L.C. Ordoñez*[2], *S. J. Figueroa-Ramírez*[1], *H.J. Mandujano-Ramírez*[1]

[1] Facultad de Ingeniería, Universidad Autónoma del Carmen, Calle 56, 4, Cd. del Carmen, Campeche. C. P. 24115, México.
[2] CONACYT-Centro de Investigación Científica de Yucatán, Parque Científico y Tecnológico de Yucatán. Carretera Sierra Papacal–Chuburna Puerto, km 5. Sierra Papacal, C.P. 97302, Mérida, Yucatán.
[*]E-mail: juanmsg@live.com.mx, jsierra@pampano.unacar.mx

Received: 2 February 2022 / *Accepted:* 14 March 2022 / *Published:* 5 April 2022

This paper presents a 3D computational fluid dynamics (CFD) study on a proton exchange membrane fuel cell (PEMFC) stack. To determine the impact of refrigeration systems on the performance of a PEMFC stack, special attention was given to sources that generate heat. The evaluated models consist of an open cathode hydrogen-air stack to which an active and passive heat dissipation system was incorporated. The general characteristics of both models were based on the designs of a commercial PEMFC. The numerical results demonstrated that the highest temperatures were presented at the cathode outlets showing a displacement towards the anode outlet. The temperature distributions were directly related to the heat sources by ohmic resistance, which mainly came from the membrane, and the entropy heat from the oxygen reduction reaction. The implementation of the heat dissipation systems effectively contributed to heat management in fuel cells. For the model with the passive heat system, ohmic heating was increased in the membrane by water formation. Regarding the model with an active system, it was possible to reduce the global temperature of the cell and reach higher current densities. This paper demonstrates that the use of the proposed cooling systems can increase the performance of a fuel cell.

Keywords: CFD, Stack modelling, PEMFCs, Heat sources.

1. INTRODUCTION

In recent years, the consumption of fossil fuels has dramatically increased due to the industrialization of developing nations and the increase in the world population. This situation has led to the need for new ways of processing and obtaining electrical energy [1]. Fuel cells (FCs) are the most

attractive alternative to provide power for transport and portable devices. Their high efficiency and low pollution levels have promoted a supply of electricity for the next generation of electric vehicles [2, 3]. In particular, proton exchange membrane fuel cells (PEMFCs) have gained more attention due to their low operating temperature and portability [4, 5]. However, both heat and water management are some of the obstacles that inhibit the achievement of higher performance, thereby further increasing the costs of fuel cells and limiting their commercialization on a large scale. [6]. If airflow removes the water from the fuel cell, the membrane-electrode assemblies (MEAs) cannot remain adequately humidified, decreasing the protonic conductivity and the power density of the fuel cell [7, 8]. On the other hand, the PEMFC generates an amount of waste heat similar to its electric power output, limiting its energy efficiency to approximately 50%. This means that the total energy released is the product of the electrical potential and produced heat. The heat generated in the PEMFC mainly stems from three sources: electrochemical reactions, ohmic heating, and vapour water condensation [9, 10].

The use of numerical methods allows the study of physical phenomena within a fuel cell, such as mass, heat and energy transport, electrode kinetics, and potential fields, that cannot be studied using only experimental techniques. Initially, the heat transfer in a PEMFC was studied with a 1-dimensional (1D), isothermal, and steady-state model. Springer et al. determined that the water diffusivity, electro-osmosis drag coefficient, and electrical conductivity were a function of the water content in the membrane [11]. Subsequently, Sivertsen and Djilali [12] developed a three-dimensional (3D) model for a single fuel cell. The model considered the distribution of generated heat associated with the electrochemical reactions in both the cathode and anode catalyst layers. Moreover, the model solved the electric and ionic potentials in the electrodes and membrane. Wang and Ouyang [13] developed a 3D model for an air-breathing PEMFC using nondimensional heat/mass transfer coefficients. In their study, they demonstrated through numerical simulation that there was a close interaction among the heat, mass transfer and electrochemical reactions in a fuel cell. On the other hand, Chen and Z. Gao [14] reported a study of optimal heat transfer in a PEMFC stack with an additional cooling plate. They proposed six cooling modes, including three serpentine-type and three parallel-type modes; the first cooling mode was better than the second. This was due to the poor distribution of cooling fluid in the parallel-type cooling mode. Liu et al. [15] simulated the first 3D model of an air-cooling mini-fuel cell stack with six cells and used different strategies to simplify their model and its mesh. Liu Z. considered a very thin homemade self-humidifying membrane with an active area of 8 cm^2 and a humidification system for air flow; also, for the purpose of their simulation, the flow fields were replaced by porous media. With their simulation results, they determined that to keep the PEMFC stack in steady operation, the fuel cell must be effectively cooled. On the other hand, Rahgoshay [16] presented a 3D computational fluid dynamics (CFD) study of a single PEM fuel cell with two types of cooling flow fields. Their results revealed that the serpentine flow field improved the index temperature by 24% compared to the parallel one, and the maximum temperature was observed at the cathode catalyst layer, particularly in the central region located at the outlet.

In this investigation, a 3D computational fluid dynamics study was developed in three PEMFC stack models without and with cooling systems (active and passive). The purpose of this study was to determine the impact of the two passive and active cooling systems on the performance of the fuel cell, as well as to estimate the contribution of the reaction and ohmic resistance heat sources. For these

models, steady state and nonisothermal conditions were assumed. First, a conventional open cathode hydrogen-air stack with ten membrane-electrode assemblies was considered as the base model. Later, two more models were made. The second model incorporated a passive heat dissipation system conformed by fins placed on the edges of the bipolar plates, while the third model included an active cooling system, including cooling channels in the bipolar plates.

2. DESCRIPTION OF THE COMPUTATIONAL MODEL

The three computational models analysed in this study consisted of a stack with nine cells connected in series. The flow fields considered in the models had a serpentine form and parallel channels for the hydrogen and air supply, respectively. The models included the membrane (MEM), gas diffusion layers (GDLs), catalyst layers (CLs), flow channels (FCHs), and bipolar plates (BPs). Fig. 1 presents the schematic configuration of the simulation domain for a PEMFC with the air supply at the cathode (conventional design). The other models are described below. The three models use two flow field patterns in the bipolar plates: serpentine in the anode and straight channels in the cathode. Table 1 presents the main design features. Fig. 2 shows a 3D view of both flow patterns cast on the bipolar plate and their dimensions.

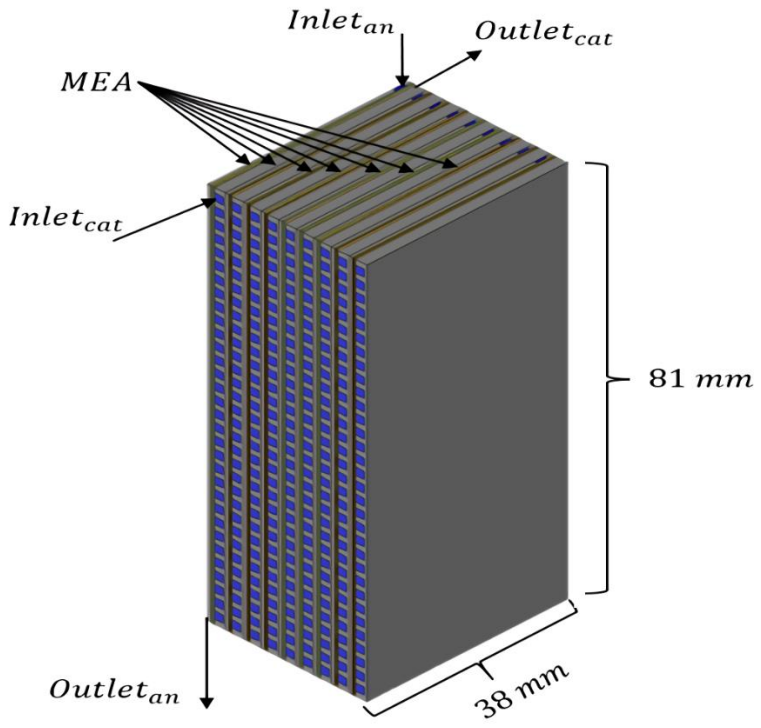

Figure 1. Schematic of a PEM fuel cell supplied with air in the cathode (conventional design).

2.1 Description of the flow patterns in the PEM fuel cell

The flow field patterns for the anode and cathode (Fig. 2) consisted of three parallel channels on a Z-type serpentine and thirty-two straight channels in parallel. The flow field supply direction was in the opposite direction for the fuel (anode) and oxidant (cathode).

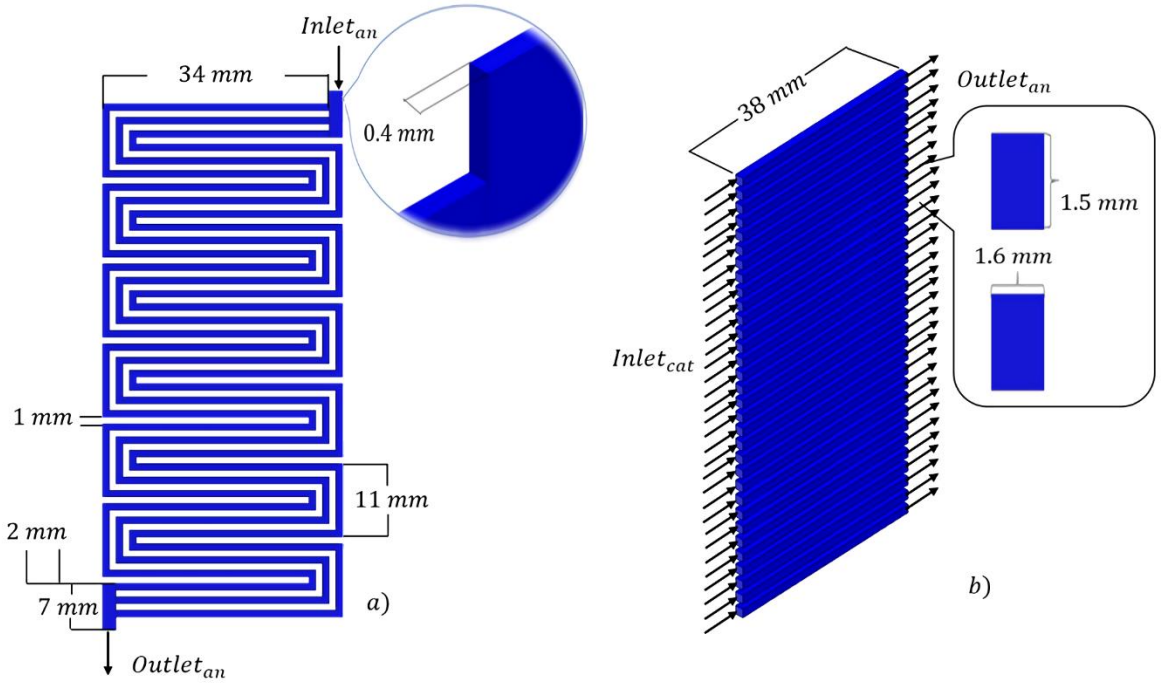

Figure 2. a) Design and dimensions of the anode flow patterns, b) cathode flow patterns.

2.2 Description of the computational model with a passive heat transfer system

In agreement with Cengel, an adequate alternative to increase the rate of heat transfer is to increase the surface area of an object by attaching fins onto it [17]. To reduce the temperature by at least 2 degrees Celsius in the PEMFC stack and to check the impact of the fins in a fuel cell, the authors calculated that the length of the fins was 17.5 mm using the equation of a rectangular fin (1). These elements were attached to the cathode outlets, where the highest temperature values were observed in the conventional design. Their location is shown in Fig. 3, and the fins material is the same as that of the bipolar plates.

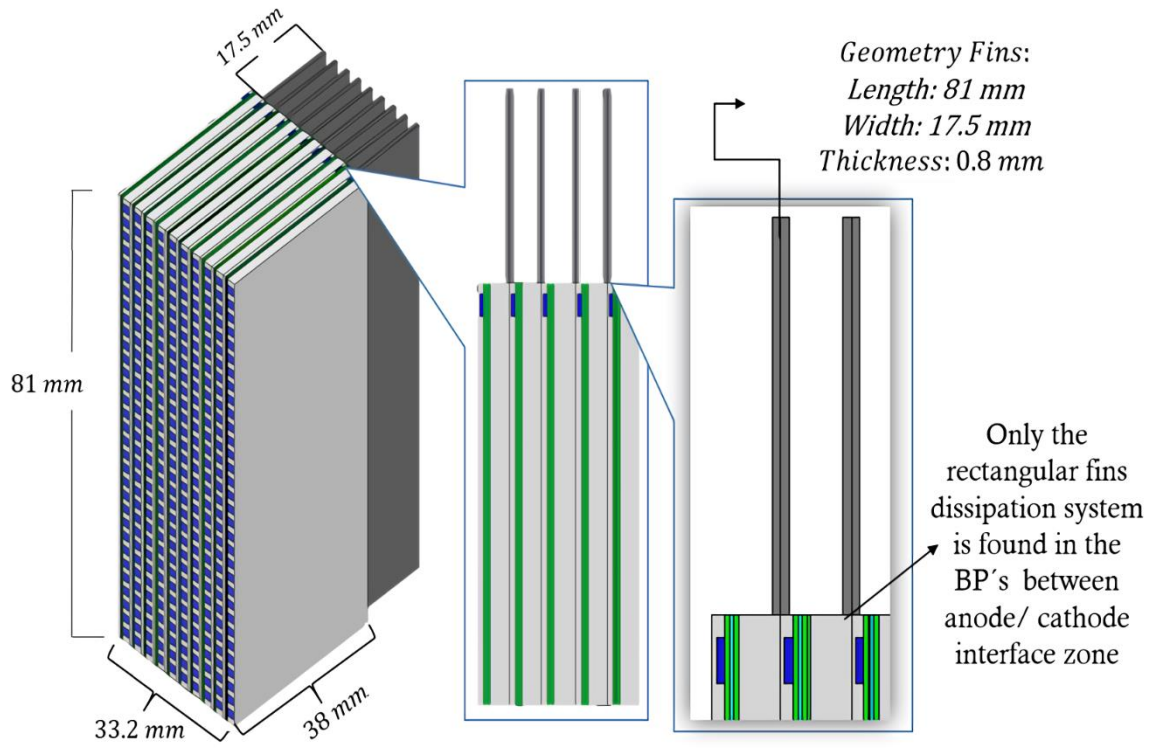

Figure 3. Schematic representation of a PEMFC stack with rectangular fins as the heat dissipation system.

2.3 Description of the computational model with cooling channels

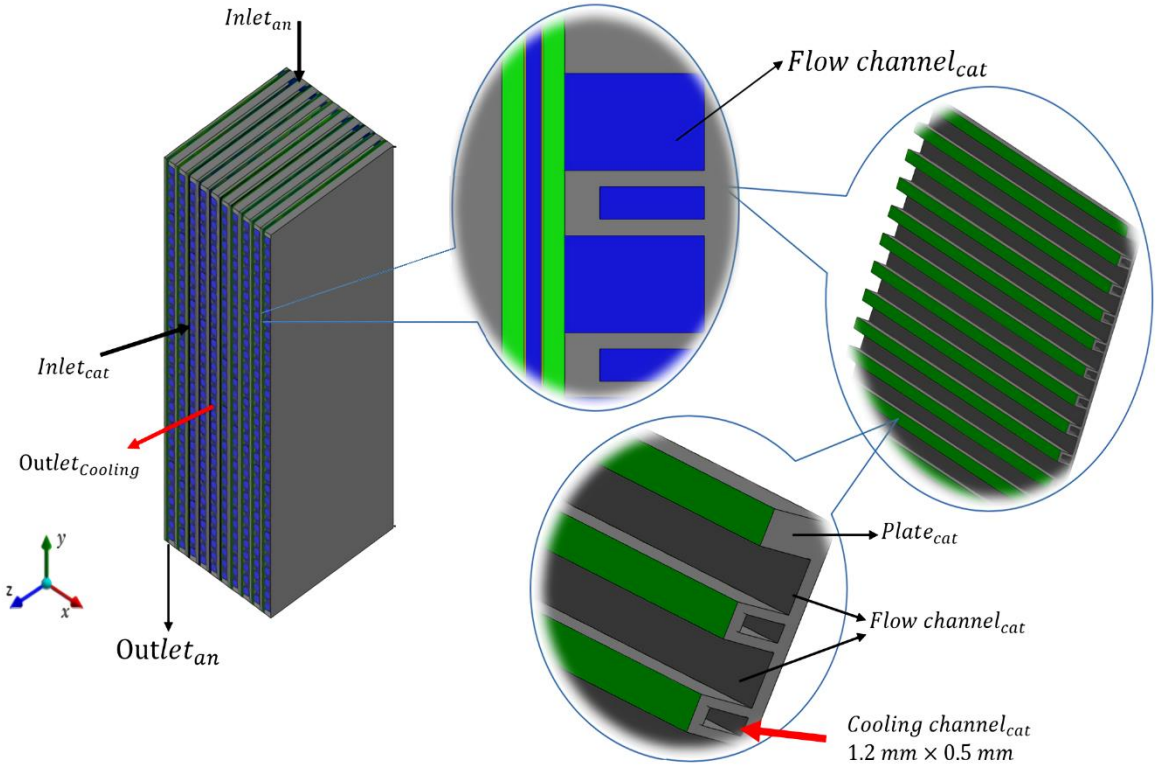

Figure 4. Schematic of the PEMFC stack and its cooling channel system in the cathode.

Since the higher temperatures achieved inside the PEMFC are presented at the cathode/membrane interface [12], the authors proposed the incorporation of cooling microchannels in the plate on the cathode side for the third model (Fig. 4). These cooling channels were straight, having a transversal section of 1.2 mm x 0.5 mm to take advantage of the shape and space on the cathodic side. Water was used as the coolant and was injected in the opposite direction to the air flow in the cathode channels.

2.4 Mesh details and considerations

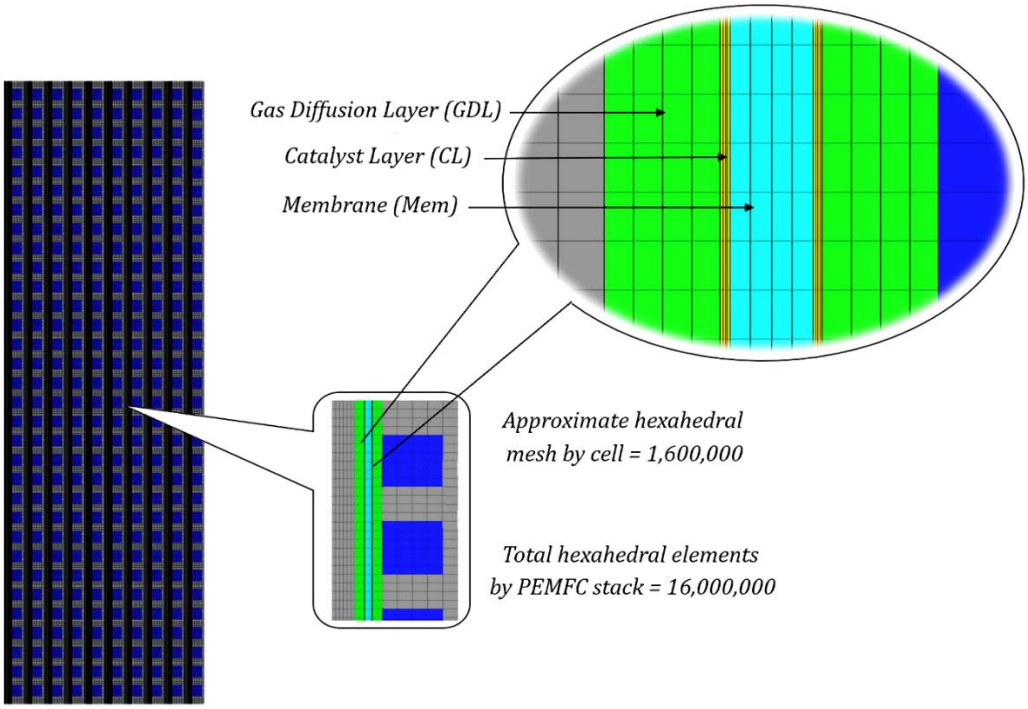

Figure 5. Mesh visualization in the domain and subdomains of the PEMFC stack models.

Table 1. Mesh dimensions and intervals of the subdomains

Subdomain	Dimensions [mm] Height × Width × Thickness	Mesh [mm] Body sizing/edge size.
Gas diffusion layer (GDL)	81 × 38 × 0.25	0.25 × 0.0625
Membrane (MEM)	81 × 38 × 0.178	0.25 × 0.045
Catalyst layer (CL)	81 × 38 × 0.02	0.25 × 0.005
Flow channel anode	N/A × 1 × 0.4	0.25 × 0.1
Flow channel cathode	N/A × 1.5 × 1.6	0.25 × 0.4
Anode plate	81 × 38 × 0.6	0.25 × 0.1
Cathode plate	81 × 38 × 2	0.25 × 0.4
Rectangular fins	81 × 17.5 × 0.8	0.25 × 0.1/0.25 × 0.4
Cooling channels (30)	81 × 38 × 0.5	0.25 × 0.4

According to a previous grid-independent study carried out by Macedo-Valencia [18], the same meshing criteria were used in this study, and the details are presented in Figure 5 and Table 1. In the case of the model with rectangular fins, a mesh refinement was made for the fins, and these were divided into two sections with a thickness of 0.4 mm. For this model, a hexahedral mesh with 17.8 million elements was constructed. For the first two models, a hexahedral mesh with approximately 16 million elements was used for each model.

3. MATHEMATICAL MODEL

To solve the computational models of the PEMFC stacks, the governing equations of computational fluid dynamics were considered; these equations were described by the authors in a previous work [19] and are summarized in Table 2. Additionally, the equations that represent the heat sources are included. To calculate the local current density distribution in the catalyst layers, the Butler-Volmer formulation was contemplated; also, to solve water transport through the membrane, the Springer correlation [11] was considered. Darcy's law was used to depict the properties of porous media (GDLs and CLs). The governing equations were discretized and solved through a CFD commercial code that used a segregated method and a SIMPLE algorithm. Likewise, a fuel cell add-on module was used to solve the PEMFC stack models [20]. To perform the simulations, potentiostatic boundary conditions were used with a potential sweep of 1 to 0.5 V.

3.1 Assumptions

The physical-chemical processes that take place inside the fuel cell were simulated by solving the conservation of charge equations and the Butler-Volmer formulation. The assumptions considered to develop the simulations were as follows:

- The PEMFC stack models are assumed to operate at a steady state.
- Nonisothermal operation and single phases in flows were considered.
- According to the Reynolds number obtained for the flows, a laminar regime was considered.
- Because gases were used in the flow channels, viscous effects were not considered in the regions near the walls.
- Electrochemical reactions took place on the surface of both electrodes.
- Gas diffusion layers and catalyst layers were considered porous isotropic media.
- The transport of liquid water in the membrane was controlled by diffusion mechanisms and electroosmotic drag.
- Taking into account the observations of Xiao-Guang [21], a temperature of 300 K was considered in this study to relieve membrane dehydration.
- Dry gases were supplied to the PEMFC stacks.

• To rule out heat attributed to interfacial phenomena by the use of very thin membranes, a Nafion 117 membrane was considered in this study.

3.2 Operating conditions and electrochemical parameters

The computational models were simulated under the operating conditions presented in Table 3. The electrochemical parameters used as boundary conditions in the membrane-electrode assemblies are shown in Table 4. The mass flow of the reactant (hydrogen) and oxidant (air) was supplied individually for each single fuel cell.

Table 2. Governing equations of the PEM fuel cell model

Fin equation	$\frac{\partial^2\theta}{\partial x^2} - a^2\theta = 0$	(1)
Continuity	$\nabla \cdot (\rho\vec{v}) = S_m$	(2)
Momentum transport	$\nabla \cdot (\rho\vec{v}\vec{v}) = -\nabla p + \nabla \cdot \left(\mu^{eff}\nabla\vec{v}\right) + S_p$	(3)
Energy	$\nabla \cdot \vec{v}(\rho E + p) = \nabla \cdot \left(k_{eff}\nabla T - \sum_j h_j\vec{J}_j \right) + S_h$	(4)
Hydrogen transport (anode)	$\nabla \cdot (\rho\vec{v}y_{H2}) = \nabla \cdot \vec{J}_{H2} + S_{H_2}$	(5)
Water transport (anode)	$\nabla \cdot (\rho\vec{v}y_{aw}) = \nabla \cdot \vec{J}_{aw} + S_{aw}$	(6)
Oxygen transport (cathode)	$\nabla \cdot (\rho\vec{v}y_{O2}) = \nabla \cdot \vec{J}_{O2} + S_{O2}$	(7)
Water transport (cathode)	$\nabla \cdot (\rho\vec{v}y_{cw}) = \nabla \cdot \vec{J}_{cw} + S_{cw}$	(8)
Charge transport	$\nabla \cdot (\sigma_{sol}\nabla\varphi_{sol}) + R_{sol} = 0$	(9)
	$\nabla \cdot (\sigma_{mem}\nabla\varphi_{mem}) + R_{mem} = 0$	(10)

Source terms

$$S_m = S_{H2} + S_{aw} \qquad S_m = S_{O2} + S_{cw} \tag{11}$$

$$S_{px} = -\frac{\mu \vec{u}}{k} \qquad S_{py} = -\frac{\mu \vec{v}}{k} \qquad S_{pz} = -\frac{\mu \vec{w}}{k} \tag{12}$$

$$\vec{J}_i = -\rho D_i \nabla \cdot y_i \tag{13}$$

$$S_h = I^2 R_{ohm} + h_{react} + \eta_{act} R_{an,ca} \tag{14}$$

$$S_{H_2} = -\frac{M_{H_2}}{2F} R_{an}\ ;\ S_{aw} = -\frac{M_{H_2O}}{F} R_{an}\ ;\ S_{O_2} = -\frac{M_{O_2}}{4F} R_{ca}\ ;\ S_{cw} = \frac{M_{H_2O}}{2F} R_{ca} \tag{15}$$

Hear sources

$$R_{an}\left(\eta_{an} - \frac{T\Delta s_{an}}{2F}\right) + \frac{i_s^2}{\sigma_{sol}} + \frac{i_m^2}{\sigma_{mem}} \qquad R_{ca}\left(-\eta_{cat} - \frac{T\Delta s_{ca}}{2F}\right) + \frac{i_s^2}{\sigma_{sol}} + \frac{i_m^2}{\sigma_{mem}} \tag{16}$$

$$\frac{i_m^2}{\sigma_{mem}} \quad (\textbf{membrane}) \qquad \frac{i_s^2}{\sigma_{sol}} \quad (\textbf{current collector}) \tag{17}$$

Table 1. Operating conditions

Pressure	P	atm	1
Cell temperature	T_c	K	300
Anode mass flow	$\dot{M}_{an}$	$kg\ s^{-1}$	3.21×10^{-7}
Cathode mass flow	$\dot{M}_{ca}$	$kg\ s^{-1}$	1.05×10^{-7}
Hydrogen mass fraction H_2, anode	X_{H_2}	-	0.9
Water mass fraction H_2O, anode	X_{H_2O}	-	0.1
Oxidant mass fraction O_2, cathode	X_{O_2}	-	0.21
Nitrogen mass fraction N_2, cathode	X_{N_2}	-	0.79
Water mass fraction H_2O, cathode	X_{H_2O}	-	0
Parameters (fin system)			
Convection heat transfer coefficient, fins.	h	$W\ m^{-2}K^{-1}$	10
Thermal conductivity	k	$W\ m^{-1}K^{-1}$	0.6
Parameters (cooling channel system)			
Coolant density	ρ	$kg\ m^{-3}$	998.2
Specific heat capacity	c_p	$J\ kg\ K^{-1}$	4182
Thermal conductivity	k	$W\ m^{-1}K^{-1}$	0.6
Dynamic viscosity	υ	$kg\ m^{-1}s^{-1}$	1.003×10^{-3}
Mass flow	$\dot{M}_{H_2O}$	$kg\ s^{-1}$	1.38×10^{-4}

Table 2. Electrochemical parameters

Ref. exchange current density (anode)	$j_{ref,an}$	$A\ m^{-2}$	7,500
Ref. exchange current density (cathode)	$j_{ref,cat}$	$A\ m^{-2}$	20
Charge transfer coefficient (anode)	α_{an}	-	2

Charge transfer coefficient (cathode)	α_{ca}	-	2
Hydrogen reference diffusivity	$D_{ref_{\mathrm{H_2}}}$	$m^2\ s^{-1}$	1.1×10^{-4}
Oxygen reference diffusivity	$D_{ref_{\mathrm{O_2}}}$	$m^2\ s^{-1}$	3.2×10^{-5}
Water reference diffusivity	$D_{ref_{\mathrm{H_2O}}}$	$m^2\ s^{-1}$	7.35×10^{-5}
Nitrogen reference diffusivity	$D_{ref_{\mathrm{N_2}}}$	$m^2\ s^{-1}$	8×10^{-5}
Concentration exponent (anode)	γ_{an}	-	0.5
Concentration exponent (cathode)	γ_{cat}	-	1
CL porosity	ε_{CL}	-	0.12
CL viscous resistance	VR_{CL}	m^{-2}	1.3×10^{12}
GDL porosity	ε_{GDL}	-	0.4
Open circuit voltage	U_{oc}	V	0.95

4. RESULTS AND DISCUSSION

The use of computational fluid dynamics techniques allows for predicting the distribution and visualization of different variables in different regions or subdomains of a model. In this section, the distribution contours, polarization curves and a graph of temperature vs. current density are presented. To determine the impact of the incorporation of cooling systems in the fuel cell stack models, the obtained results are analysed and discussed below.

4.1 Base model validation

To guarantee the reliability of the simulation results, the conventional design (base model) was simulated and compared with the numerical results reported by Macedo-Valencia [18]. Macedo-Valencia et al. validated their model with experimental data showing a good correlation of results. In the present study, the PEMFC stack models included ten cells connected in series, an active area of 24 cm^2, and an air flow supplied individually to each cell; therefore, the gas inlets and mass fractions were recalculated as shown in Table 3. Likewise, as seen in Fig. 6 of this study, the current density range of the polarization curve was extended to 0.35 A/cm^2, this allowed us to more clearly appreciate the potential drop resulting from mass transport losses.

It is worth noting that this polarization curve corresponds to a model based on a commercial fuel cell (Horizon H-100), which was supplied with dry flows of hydrogen and air as reactants. Additionally, normal operating conditions of 1 atm and 300 K were considered, as in the experimental tests. Therefore, the performance of the base model was lower than that of common polarization curves obtained in experimental fuel cells that were supplied with pure oxygen and were evaluated under optimal operating conditions (353 K, 3 atm, RH 100%) and those utilizing Nafion 212 membranes, among others. In this way, the numerical results of this study were compared under the same criteria considered by Macedo-Valencia in experimental tests. In addition, the potential obtained for the base model was averaged over ten cells, and the current density was given per unit area.

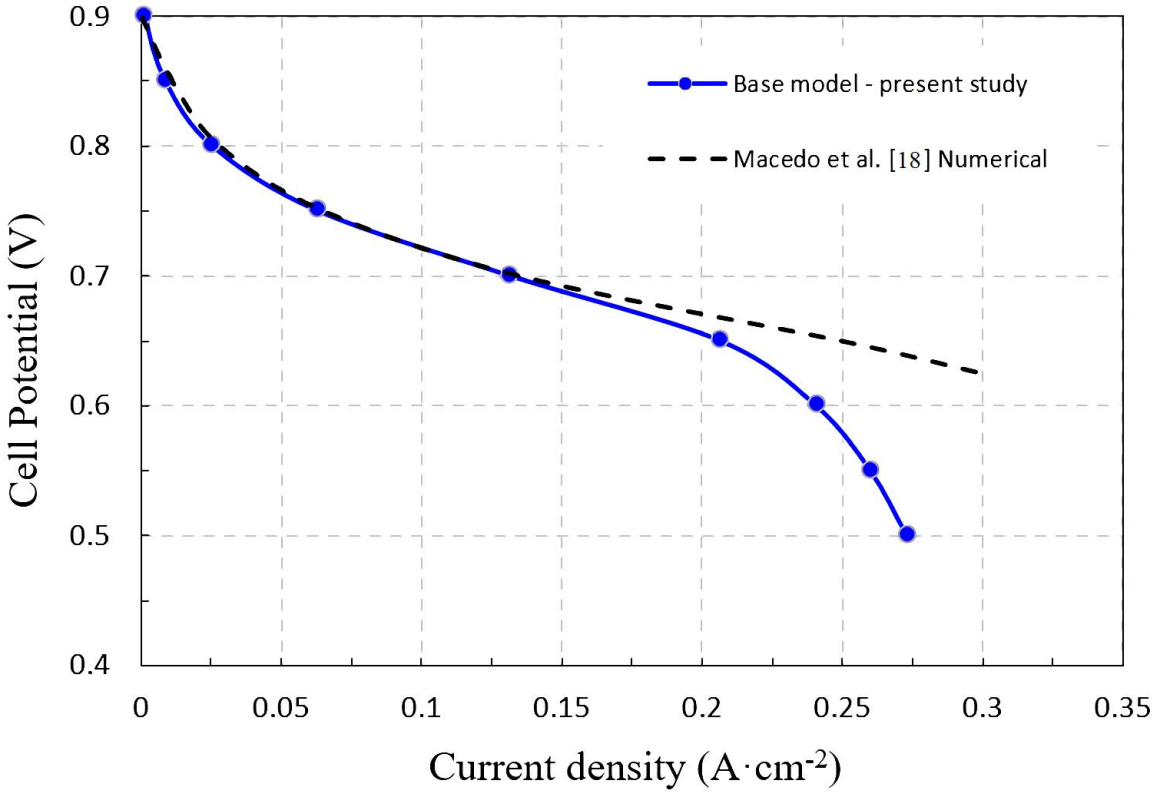

Figure 6. Comparison between the base model and numerical results reported by Macedo-Valencia [18].

4.2 Oxygen and water mass fraction distributions

The oxygen and water concentration distributions are key factors for optimal fuel cell performance because the activation and concentration overpotentials are related to their consumption and production rates at the cathode [22]. Figure 7 shows the distribution of the oxygen (left) and water (right) mass fractions in the cathode catalyst layer for the three models of the PEMFC stack. These contours corresponded to a potential of 0.6 V, which was the potential at which the three models produced their maximum power. As observed in Fig. 7 (a), the oxygen concentration (left) gradually decreased in the catalyst layer from the inlet to the outlet of the cathode channels. As the supplied air moved through parallel channels, oxygen was immediately consumed in the first half of the catalyst layer; on the other hand, the water concentration (right) gradually increased in the opposite way from the inlet to the outlet due to oxygen consumption and water production rates of the electrochemical reactions.

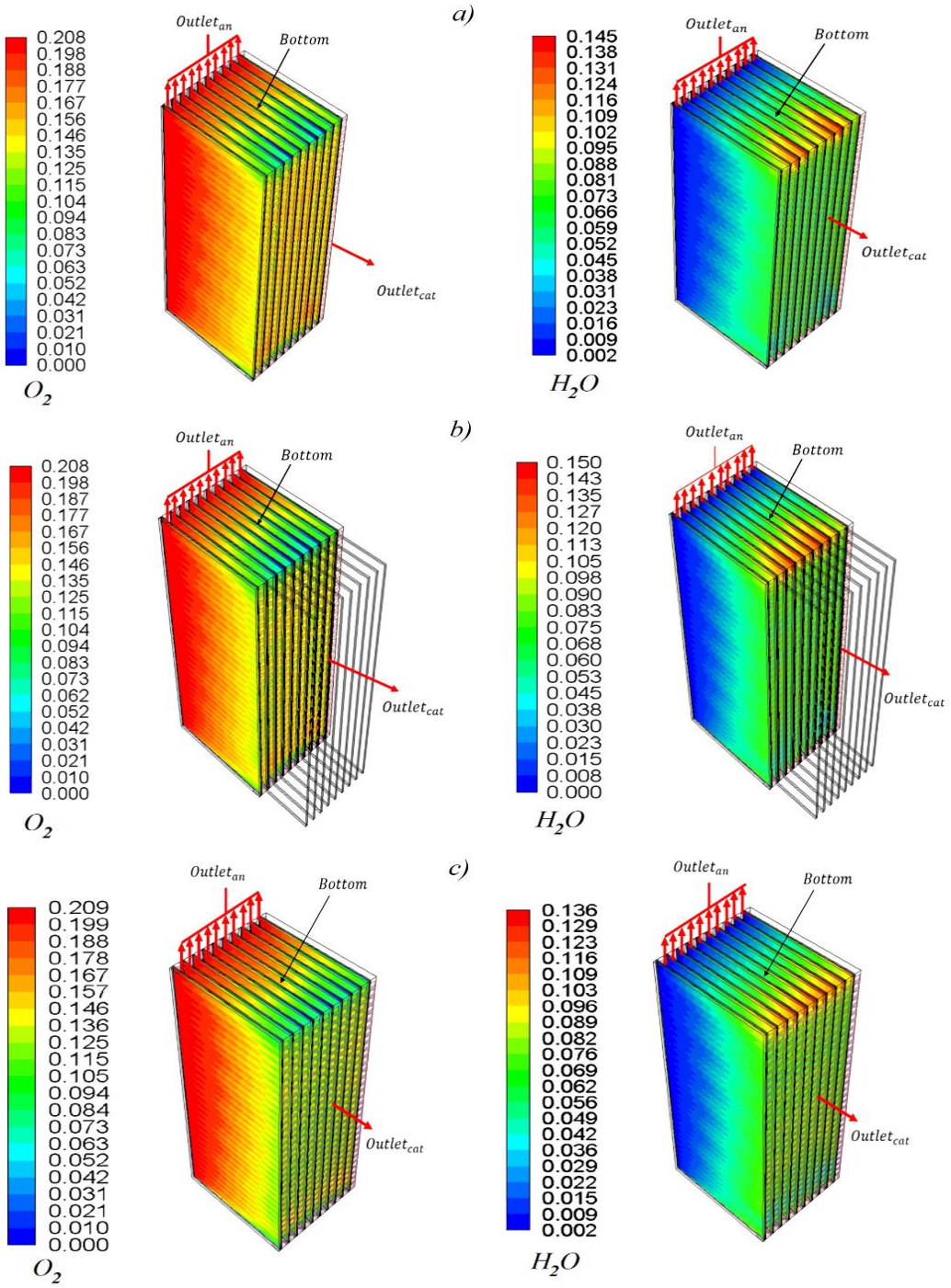

Figure 7. Oxygen and water mass fraction distributions for different PEMFC models at 0.6 V: (a) conventional design (b) stack with rectangular fins and c) stack with cooling channels.

The water concentration increased in the region where both the anode and cathode outlets were located, with two characteristic red crests being observed in MEAs #3 and #4 and #7 and #8. A similar phenomenon was reported by Shimpalee for a short PEMFC stack with six cells [23]. The downstream water concentration increased due to the dragging caused by the airflow direction. In addition, another advantage of the use of straight channels for the supply of air to the cathode was that it did not result in high pressure drops [24].

In the case of the PEMFC stack with rectangular fins Fig. 7 (b), the oxygen distribution pattern and the magnitude of the oxygen concentration were similar to those of the conventional model. However, in the case of the water concentration, there was a slight increase in the magnitude of the water concentration from 0.145 to 0.150; therefore, although the variation in this parameter was small for this interface, the incorporation of rectangular fins caused a positive impact on water management, which will be discussed later for its relationship with other parameters.

Regarding the model with cooling channels shown in Fig. 7 (c), the concentrations of oxygen (left) and water (right) presented a distribution pattern similar to the previous models; however, it is important to note that the low oxygen concentration (blue crests) in the model with the conventional design shown in the figure at the bottom did not stand out as much as the model with cooling channels. Notably, the amplitude of the crests were slightly wider for the latter, which meant a greater utilization of oxygen for MEAs #3 and #4 and #7 and #8; however, this also caused MEAs #5 and #6 to show a reduction in oxygen concentration in this region. The water concentration also presented similar behaviour, resulting in a more uniform distribution than the other models; thus, the highest water concentration values also decreased from 0.150 to 0.136 compared to the previous model. This variation, although it may seem small, was important since it would be directly reflected in ohmic heating.

4.3 Heat source distributions

The heat generated in a fuel cell that is not used for a phase change is due to two main causes, namely, reaction heat sources and ohmic heating; however, the greatest heat input produced by these sources was due to the oxygen reduction reaction (ORR) [25]. The following figures show the distribution contours of the heat sources by reaction (left) and ohmic heating (right) at the GDL-CL and MEM-CL interfaces, respectively, both of which are on the cathode side. The results for the conventional PEMFC stack are shown in Fig. 8 (a). For this stack, the heat source manifested itself with greater intensity in MEAs #4 and #7. These distribution patterns matched the water concentration distributions because the speed of the electrochemical reactions was directly related to the water activity of the membrane [26]. The consumption of oxygen and water formation in this zone promoted a more efficient reaction that was reflected in the higher current density peaks; this was also reported by Ju. Just as the water formation on the cathode helped to keep the membrane fully hydrated, it also increased the heat generated by the transport of protons due to ohmic heating. Since the water activity was higher under the ribs of the bipolar plate than in the channels [27], ohmic heating also occurred in these zones. Additionally, greater water activity favoured the transport of protons from the anode to the cathode and therefore generated more heat, which was transported to the plates. As observed in Fig. 8 (b), the highest values of ohmic heating occurred in MEAs #4, #5, #6 and #7 due to stack symmetry and because more heat was generated in the centre of the fuel cell.

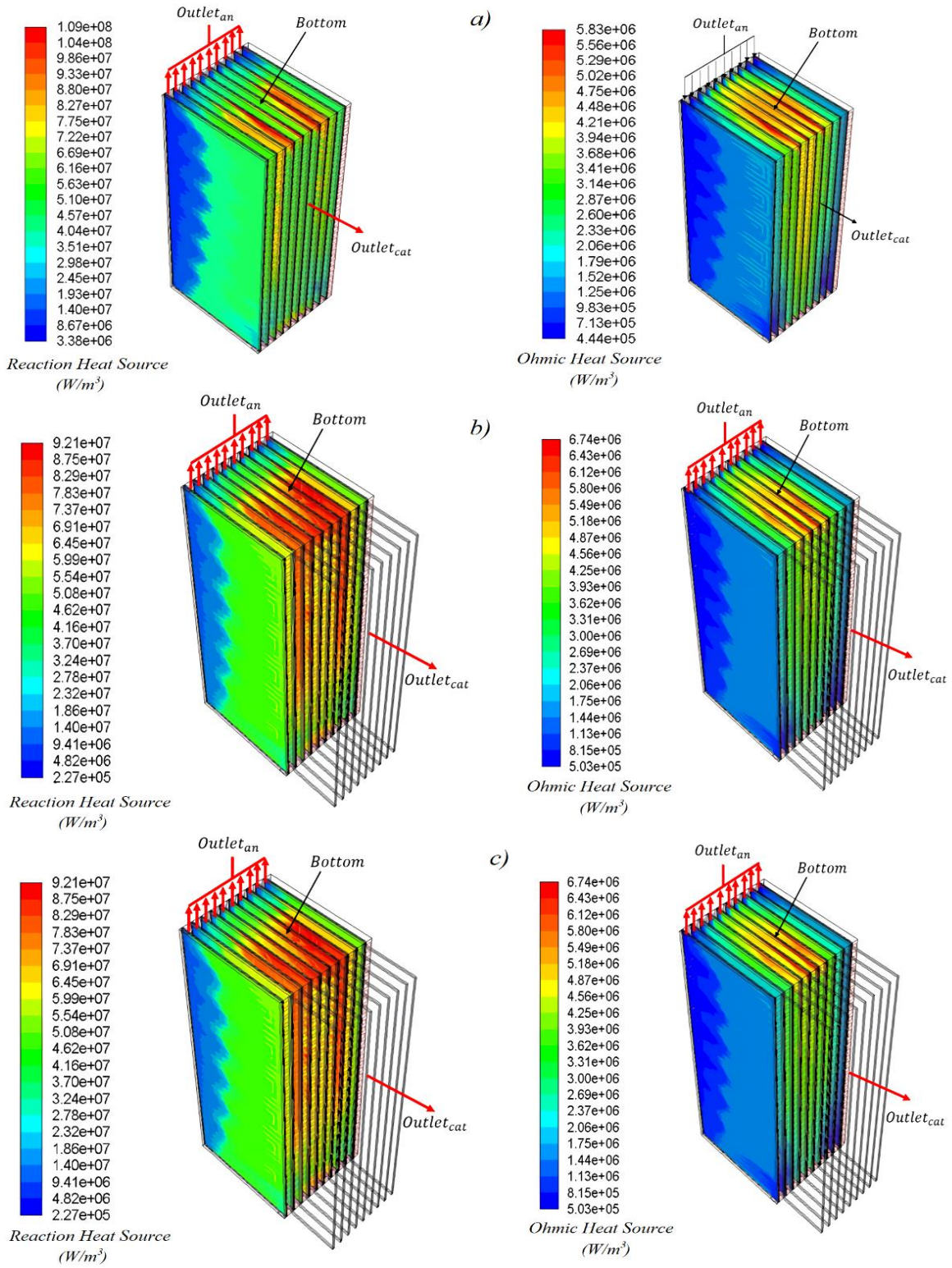

Figure 8. Heat source distributions for different PEMFC models at 0.6 V: (a) conventional design (b) stack with rectangular fins and c) stack with cooling channels.

On the other hand, for the model with rectangular fins, similar behaviour was observed in Fig. 8 (b); the contours were more distributed than in the case of conventional design. Although the intensity of the red colour showed a greater effect, the magnitude of the reaction heat sources were smaller (1.09

x 10^8 vs. 9.27 x 10^7 W/m^3). The use of fins promoted the removal of heat generated by the ORR, which was ~15% lower than that of the conventional model. However, even though the model with fins managed to reduce the heat generated by the reaction, the ohmic heating in the membrane was 15% higher. This might seem discouraging or neutral while analysing these processes locally, but globally, the stack temperature was reduced with the addition of fins, as will be seen later.

The results of the stack with cooling channels are shown in Fig. 8 (c). The heat sources by reaction presented a value 4% lower than the conventional model, and the heat distribution was even more uniform than in the other two models, which showed that the incorporation of cooling channels evenly distributed the heat over a wider region of the fuel cell, which included at least six of the central bipolar plates (left); therefore, higher heat dissipation was achieved. In the case of ohmic heat sources (right), similar behaviour was observed, and the heat was distributed mainly in the four central plates of the stack. For this model, the ohmic heat generation was 4% less than that of the conventional model; therefore, it was the model that, on average, dissipated the greatest heat from the cell.

The passive heat dissipation system aided in dissipating the heat generated at the cathode, which allowed the membrane to stay more hydrated; however, a higher water content in the membrane increased its ionic conductivity, and therefore, the heat due to ohmic resistance was higher. Table 3 shows the sources of generated heat in the three PEMFC stack models and the contribution of each model.

Table 3. Maximum heat sources by the PEMFC stack models with/without a heat dissipation system.

PEMFC stack models	Maximum reaction heat sources CL_{cat} $\mathrm{W/m^3}$	Maximum ohmic heat sources $\mathrm{Mem_{cat}}$ $\mathrm{W/m^3}$
Conventional PEMFC stack	1.09×10^8	5.83×10^6
PEMFC stack with rectangular fins	9.21×10^7	6.74×10^6
PEMFC stack with cooling channels	1.05×10^8	5.57×10^6

The heat generated by the oxygen reduction reaction for the conventional model presented the highest values compared to the proposed models. The stack with rectangular fins mainly removed the heat generated by the ORR from the cathode catalyst layer, which represented approximately 80 to 90% of the total waste heat released from the PEMFC [25], but not the heat by the ohmic resistance from the membrane. The model with cooling channels was more efficient in heat removal, and the water that was injected as coolant allowed for better distribution of the heat inside the cell and further reduced the overall temperature of the stack.

4.3 Current density distribution

Fig. 9 presents the current density contours of the three stack models. The current density contours were obtained from the cathode catalyst layers because it was possible to observe the areas in which higher energy demand of the stack was subject in these regions, and this demand was directly related to the water concentration distribution and heat resources. The results showed that the current density was extracted by the bipolar plates through the ribs and not from the areas above the channels [29]. Its distribution pattern was reflected in the cathode catalyst layers (CLCs), and this distribution was a function of the mass and energy transport processes mentioned above. For the conventional model, CCLs #3, #4, #7 and #8 presented the highest current density values. For the model with rectangular fins, the current density manifested with greater intensity towards the centre of the stack, specifically CCLs #4, #5, #6, #7, and #8. On the other hand, for the model with cooling channels, although high current density peaks were not manifested, the highest current intensity converged towards the central CCLs of the stack. It is worth mentioning that this model presented the highest values of current density compared to the previous two.

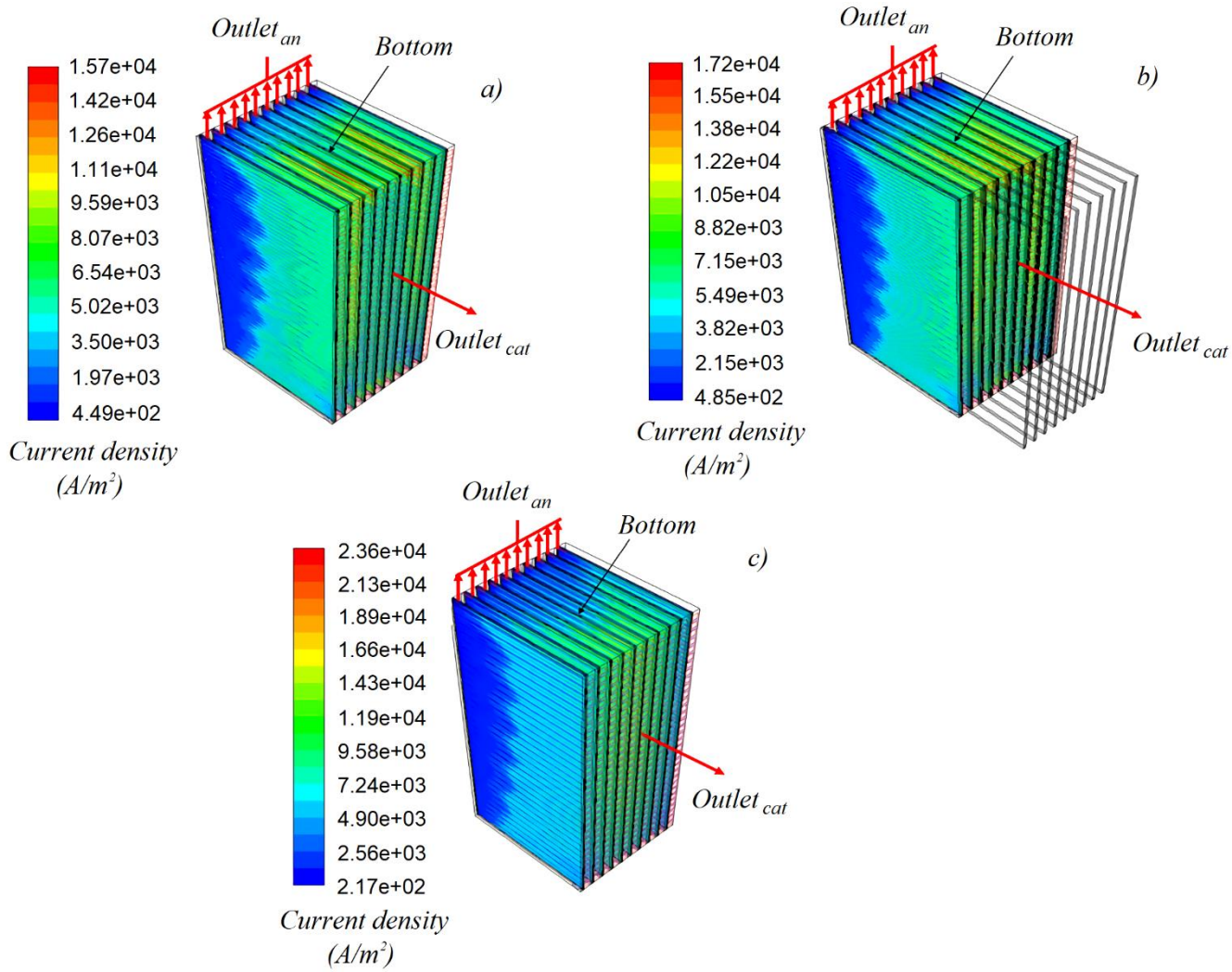

Figure 9. Current density distributions for different PEMFC models at 0.6 V: (a) conventional design, (b) model with rectangular fins and (c) model with cooling channels.

4.2 Temperature distribution

Regarding the temperature distribution, the following figures show the distribution contours of the three stack models.

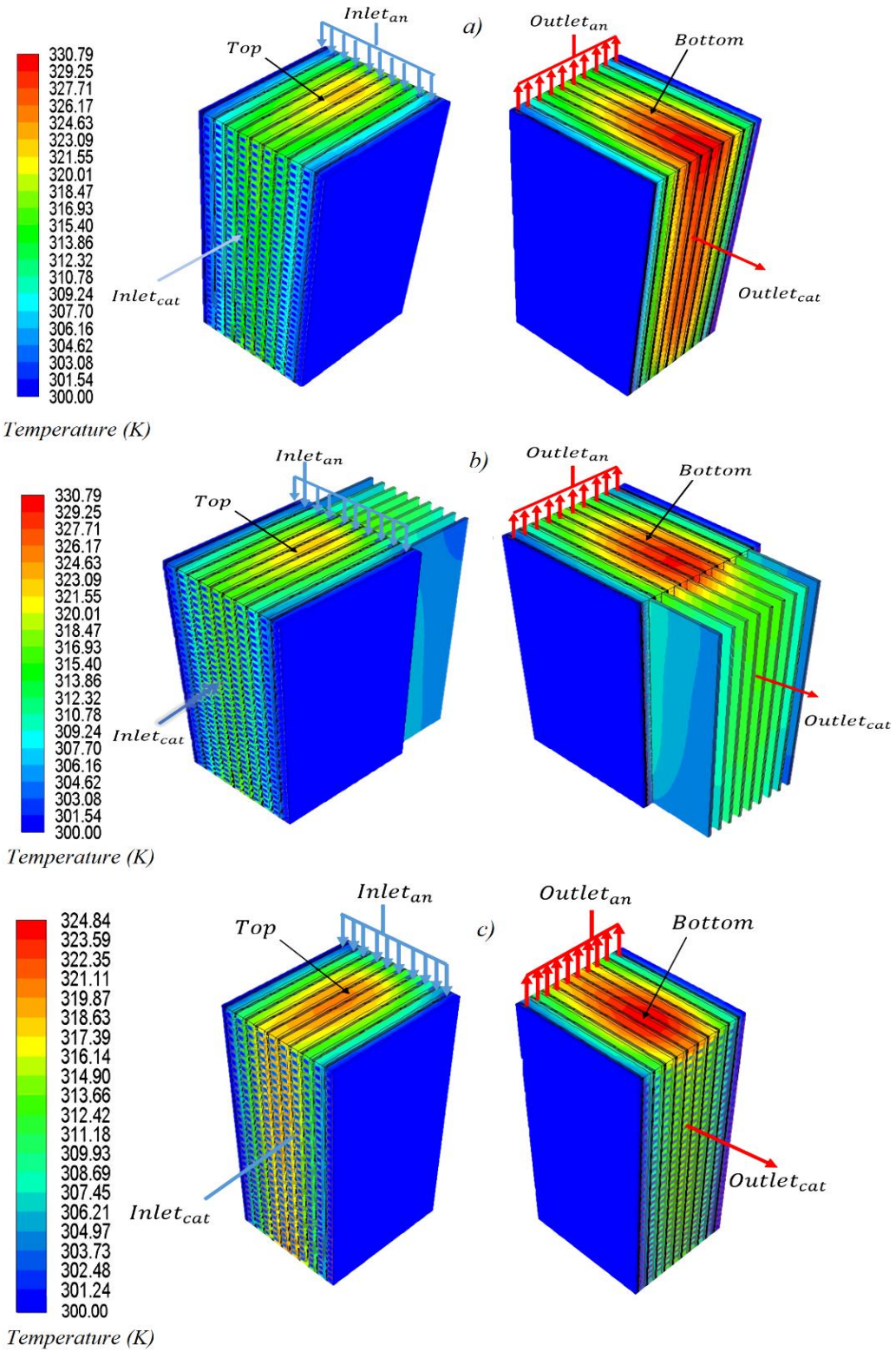

Figure 10. Temperature distributions for different PEMFC models at 0.6 V: (a) conventional design, (b) model with rectangular fins and (c) model with cooling channels.

The results are presented in the bipolar plates because it is fast and easy to validate them with experimental data [18]; however, the highest temperature in the PEMFC stack was observed in the catalyst layers due to the electrochemical reaction and ohmic heating. For the conventional stack model (Fig. 10), the highest temperature values occurred at the cathode outlet, particularly in the central plates and with an orientation towards where the hydrogen outlet was located (below). This indicated that much of the heat generated in the cell was effectively removed through the bipolar plates, but the design and orientation of the flow fields also exhibited significant contributions. These results coincided with those reported by Macedo-Valencia, who also experimentally validated his results. For the model with rectangular fins, the same temperature distribution pattern was observed; however, the fins played an important role and clearly helped transport some of the heat out of the stack. Although the default temperature scale marked the same temperature range as the conventional model at a potential of 0.6 V, when the average temperature in each stack (without fins) was calculated, the overall temperature of the stack decreased by approximately 2 K in the model with rectangular fins. For the model with cooling channels, a high temperature was only observed near the hydrogen outlet and in the central plates of the stack. The heat that manifested itself in the air outlet was considerably reduced, and the maximum temperature decreased by at least 5 K for this model. The use of cooling channels removed heat more effectively than the rectangular fins.

Finally, to complement the numerical results, the polarization curves obtained by simulation with a potential sweep from 0.95 to 0.5 V are presented below. Likewise, as the current densities were obtained, the maximum temperature values presented by the three stack models were also recorded. As seen in Fig. 11, at high potentials where the activation potential was predominant, no model showed significant differences. However, from 0.75 V, when significant current densities began to be generated and ohmic losses were important, the graphs began to separate. The curves of the models with heat dissipation systems remained above the curve of the conventional model beginning at 0.65 V. Here, the mass transport losses contributed to the slope of the three curves, causing them to change significantly; thus, both models presented higher current densities than the conventional model.

In addition, Fig. 12 shows the maximum temperature values as a function of the current density generated by the three PEMFC models. As seen in the graphs for a given current density, a significant temperature gradient was obtained for each model of the PEMFC stack. The conventional model presented the highest temperatures in the entire current density range. The models with heat dissipation systems (model with heat dissipation fins and model with cooling channels) presented average temperature decreases of approximately 4 and 8 K, respectively.

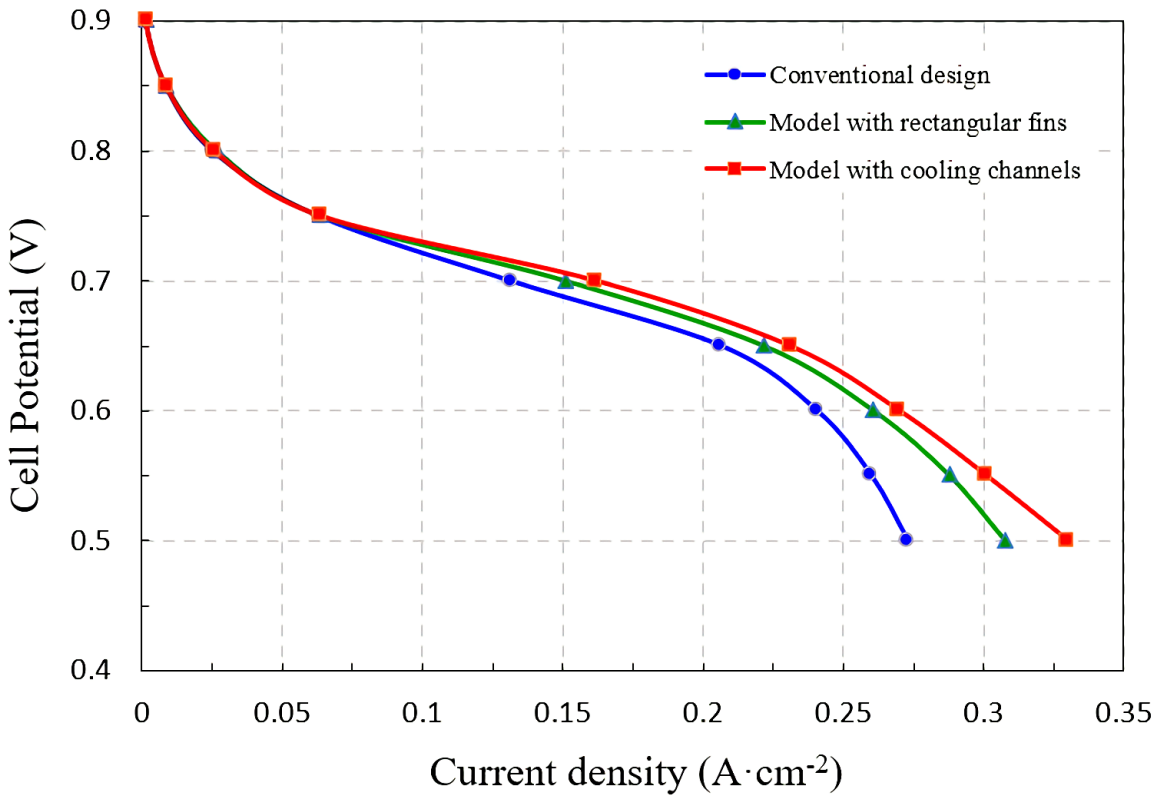

Figure 11. Polarization curves obtained of the three PEMFC stack models.

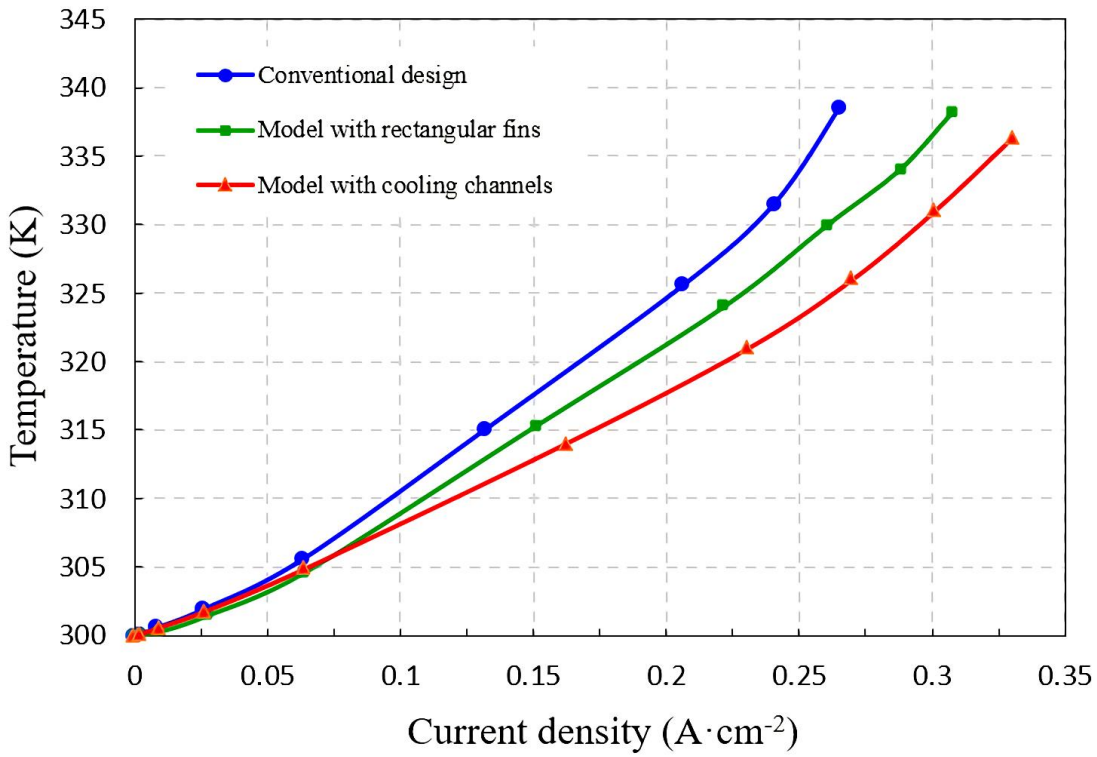

Figure 12. Maximum temperature increase vs. current density in the PEMFC stacks with/without different heat dissipation systems.

Therefore, it was evident that the proposed heat dissipation systems considerably decreased the stack temperature, which was mainly contributed by the mass transport processes. Each heat dissipation system provided different heat distribution mechanisms, but the model of the PEMFC stack with the cooling channels managed to decrease by up to 12 K at a maximum current density of 0.27 A/cm^2. Nevertheless, the use of an auxiliary device for the supply of water or some refrigerant implied a global energy load, so it would have to be evaluated until the scales could be profitable.

4. CONCLUSION

In this study, a three-dimensional heat transfer numerical assessment of two heat dissipation systems was developed using CFD for a PEMFC. The numerical results demonstrated that the orientation of the flow fields influenced the rates of consumption and production of species, which was reflected in the distribution of heat from the oxygen reduction reaction (ORR) at the cathode and the ohmic heat in the membrane. This resulted in causing a thermal imbalance in the bipolar plates of the fuel cell stack. The implementation of heat dissipation systems contributed to controlling the heat generated in a fuel cell. The passive system (rectangular fins) promoted the removal of heat generated by the ORR through the bipolar plates, slightly lowering the temperature of the central zone of the stack. However, this region also showed the highest concentration of water generated at the cathode, which also promoted greater ionic transport and greater heating due to the Joule effect. On the other hand, the active system (cooling channels) decreased both the heat generated by the reaction and Joule effect, which allowed us to reduce the global temperature of the stack and obtain higher current densities. The efficiency of the PEMFC with cooling channels was 6% higher than that of the conventional model. Therefore, proper heat management in the stacks had a positive influence on the mass and energy transport processes and therefore on the overall performance of the fuel cell.

ACKNOWLEDGEMENT
The authors acknowledge CONACyT for the financial support from Project 254667 “Consolidación del Laboratorio de Energía Renovable del Sureste (LENERSE)”.

References

1. N. L. Panwar, S.C. Kaushik, and S. Kothari, *Renew. Sust. Energ. Rev*. 15 (2011) 1513.
2. H. Rezk, A. M. Nassef, A. H. Alami, and A. Fathy, *Int. J. Hydrogen Energy*, 46 (2021) 6110.
3. C. H. Zheng, C. E. Oh, Y. I. Park, and S. W. Cha, *Int. J. Hydrogen Energy*, 37 (2012) 1790.
4. EG&G Technical Services, Inc., Fuel cell handbook, (2004) Department of Energy, U.S.
5. F. Barbir, PEM Fuel Cells – Theory and Practice, 2nd Edition, Academic Press, *Elsevier*, (2012) California, USA.
6. Z. Yang, Q. Du, Z. Jia, C. Yang, and K. Jiao, *Energy*, 183 (2019) 462.
7. J. Lee, M. H. Gundu, N. Lee, K. Lim, S. W. Lee, and H. Ju, *Int. J. Hydrogen Energy*, 45 (2020) 11704.
8. G. Guvelioglu and H. G. Stenger, *J. Power Sources*, 163 (2007) 882-91.
9. S. G. Kandlikar and Z. Lu, *Applied Thermal Eng.*, 29 (2009) 1276.

10. H Ju, H. Meng and C. Y. Wang, *Int. J. Heat Mass Transfer*, 48 (2005) 1303.
11. T. E. Springer, T. A. Zawodzinki, and Gottesfeld, *J. Electrochem. Soc*., 138 (1991) 2334.
12. N. Djilali and L. Donming, *Int. J. Therm. Sci*., 41 (2002) 29.
13. Y. Wang and M. Ouyang. *J. Power Sources*, 164 (2007) 721.
14. F. Chen, Z. Gao, R. O. Loufty, and M. Hecht, *Fuel Cells*, 3 (2003) 181.
15. Z. Liu, Z. Mao, C. Wang, W. Zhuge and Y. Zhang, *J. Power Sources*, 160 (2006) 1111.
16. S. Rahgoshay, A. Ranjbar, A. Ramiar, and E. Alizadeh, *Energy,* 134 (2017) 61.
17. Y. Cengel. Heat and Mass Transfer: Fundamentals and Applications, 4th Edition, Mc-Graw Hill, 2010.
18. J. Macedo, J. M. Sierra, S. J. Figueroa, S. E. Díaz, and M. Meza, *Int. J. Hydrogen Energy*, 41 (2016) 23425.
19. J. M. Sierra, S. J. Figueroa, S. E. Díaz, J. Vargas, P. J. Sebastian, *Int. J. Hydrogen Energy*, 39 (2014) 16694.
20. ANSYS Inc., Fluent Fuel Cell Modules Manual, (2013), Pensilvania U.S.A.
21. Y. Xiao-Guang, Q. Ye, and P. Cheng, *Int. J. Hydrogen Energy, 36* (2011) 12524.
22. L. Nuñez-Toledo, S. Castañeda, D. C. Orozco-Gallo, R. Ribadeneira, *Electrochim. Acta* 331 (2020) 135361.
23. S. Shimpalee, M. Ohashi, J. W. Van Zee, C. Ziegeler, C. Stoeckmann, C. Sadeler, C. Hebling, *Electrochim. Acta*, 54 (2009) 2899.
24. K. N. Kim, D. H. Jeon, J. H. Nam, B. M. Kim, *Int. J. Hydrogen Energy*, 37 (2012) 9212.
25. J. Hyunchul, M. Hua, and W. Chao-Yang, *Int. J. Heat Mass Transfer* 48 (2005) 1303.
26. E. Afshari and S. A. Jazayeri, *Am. J. Appl. Sci*. 6 (2009) 101-108.
27. C. E. Hernández, S. J. Figueroa, H. Mandujano, L. Santis and J. M. Sierra. *Int. J. Electrochem. Sci*. 15 (2020) 12654.